

# Toward measuring supermassive black hole masses with interferometric observations of the dust continuum<sup>⋆</sup>

GRAVITY Collaboration: A. Amorim<sup>15,17</sup>, G. Bourdarot<sup>1</sup>, W. Brandner<sup>18</sup>, Y. Cao<sup>1,\*\*</sup>, Y. Clénet<sup>2</sup>, R. Davies<sup>1</sup>, P. T. de Zeeuw<sup>1,13</sup>, J. Dexter<sup>20,1</sup>, A. Drescher<sup>1</sup>, A. Eckart<sup>3,14</sup>, F. Eisenhauer<sup>1</sup>, M. Fabricius<sup>1</sup>, N. M. Förster Schreiber<sup>1</sup>, P. J. V. Garcia<sup>11,16,17</sup>, R. Genzel<sup>1,4</sup>, S. Gillessen<sup>1</sup>, D. Gratadour<sup>2,21</sup>, S. Hönig<sup>5</sup>, M. Kishimoto<sup>6</sup>, S. Lacour<sup>2,12</sup>, D. Lutz<sup>1</sup>, F. Millour<sup>7</sup>, H. Netzer<sup>8</sup>, T. Ott<sup>1</sup>, T. Paumard<sup>2</sup>, K. Perraut<sup>9</sup>, G. Perrin<sup>2</sup>, B. M. Peterson<sup>22</sup>, P. O. Petrucci<sup>9</sup>, O. Pfuhl<sup>12</sup>, M. A. Prieto<sup>19</sup>, D. Rouan<sup>2</sup>, D. J. D. Santos<sup>1</sup>, J. Shangguan<sup>1,\*\*</sup>, T. Shimizu<sup>1</sup>, A. Sternberg<sup>8,10</sup>, C. Straubmeier<sup>3</sup>, E. Sturm<sup>1</sup>, L. J. Tacconi<sup>1</sup>, K. R. W. Tristram<sup>11</sup>, F. Widmann<sup>1</sup>, and J. Woillez<sup>12</sup>

(Affiliations can be found after the references)

Received 1 August 2022 / Accepted 28 September 2022

#### **ABSTRACT**

This work focuses on active galactic nuclei (AGNs) and on the relation between the sizes of the hot dust continuum and the broad-line region (BLR). We find that the continuum size measured using optical/near-infrared interferometry (OI) is roughly twice that measured by reverberation mapping (RM). Both OI and RM continuum sizes show a tight relation with the H $\beta$  BLR size, with only an intrinsic scatter of 0.25 dex. The masses of supermassive black holes (BHs) can hence simply be derived from a dust size in combination with a broad line width and virial factor. Since the primary uncertainty of these BH masses comes from the virial factor, the accuracy of the continuum-based BH masses is close to those based on the RM measurement of the broad emission line. Moreover, the necessary continuum measurements can be obtained on a much shorter timescale than those required monitoring for RM, and they are also more time efficient than those needed to resolve the BLR with OI. The primary goal of this work is to demonstrate a measuring of the BH mass based on the dust-continuum size with our first calibration of the  $R_{BLR}$ - $R_d$  relation. The current limitation and caveats are discussed in detail. Future GRAVITY observations are expected to improve the continuum-based method and have the potential of measuring BH masses for a large sample of AGNs in the low-redshift Universe.

Key words. galaxies: active – galaxies: nuclei – quasars: supermassive black holes – galaxies: Seyfert

#### 1. Introduction

Measuring the mass of supermassive black holes (BHs) is challenging as this requires resolving stellar or gas dynamics inside the BH sphere of influence (e.g., Thomas et al. 2004; Onken et al. 2014; Saglia et al. 2016; Hicks & Malkan 2008; Davis 2014; Onishi et al. 2017; Boizelle et al. 2019). In active galactic nuclei (AGNs) with broad recombination lines, the reverberation mapping (RM) method has been developed to measure the size of the broad-line region (BLR) and hence lead to the measurement of the BH mass (Blandford & McKee 1982; Peterson 1993; Peterson et al. 2004). By monitoring the variability of the UV/optical continuum and an emission line, typically  $H\beta$ , the BLR size can be obtained from the RM method. Assuming that the BLR is a virialized system, we can calculate the BH mass,

$$M_{\rm BH} = f \frac{R_{\rm BLR} (\Delta V)^2}{G},\tag{1}$$

where  $R_{\rm BLR}$  is the BLR radius,  $\Delta V$  is the velocity width of the broad emission line, f is the corresponding virial factor, and G

is the gravitational constant. The full width at half maximum (FWHM) or second moment ( $\sigma_{\text{line}}$ ) of the broad line is commonly used as  $\Delta V$ . The virial factor f depends on the geometry, kinematics, and inclination of the BLR clouds and is likely different from object to object. For example, the virial factor is 0.75 assuming an isotropic velocity distribution of Keplerian motion (Netzer et al. 1990). The mean virial factor,  $\langle f \rangle$ , can be calibrated using nearby AGNs, assuming that the AGN and quiescent galaxies follow the same  $M_{\rm BH}$ – $\sigma_*$  relation (e.g., Onken et al. 2004; Woo et al. 2010; Graham et al. 2011; Grier et al. 2013; Ho & Kim 2014). This method, based on RM measurements, has been used successfully for many years, despite potential biases and caveats in the calibration of the virial factor (Shankar et al. 2019). For a particular source, the uncertainty in f may come from its unknown inclination angle and other effects such as the radiation pressure (Collin et al. 2006; Mejía-Restrepo et al. 2018).

Moreover, a scaling relation between the BLR radius and AGN luminosity was discovered from RM measurements (Kaspi et al. 2000; Dalla Bontà et al. 2020, and references therein). This *R–L* relation enables estimating the BH mass only with the AGN luminosity and the FWHM of a broad emission line from single-epoch spectra (Shen 2013). Because it is simple, the single-epoch method has been widely used with different broad lines in the UV and optical, although the uncertainty is about 0.5 dex or higher (e.g., Vestergaard & Peterson 2006). Other methods have been developed to estimate the BH mass and were tested against the RM-measured BH mass. For example, the coronal

<sup>\*</sup> GRAVITY is developed in a collaboration by the Max Planck Institute for Extraterrestrial Physics, LESIA of Observatoire de Paris/Université PSL/CNRS/Sorbonne Université/Université de Paris and IPAG of Université Grenoble Alpes/CNRS, the Max Planck Institute for Astronomy, the University of Cologne, the CENTRA – Centro de Astrofisica e Gravitação, and the European Southern Observatory.

\*\* Corresponding authors: J. Shangguan, e-mail: shangguan@mpe.mpg.de and Y. Cao, e-mail: ycao@mpe.mpg.de.

line [Si VI]1.963  $\mu$ m can be used to estimate the BH mass with an uncertainty of about 0.5 dex (Prieto et al. 2022).

Recently, the BLRs of three AGNs have been spatially resolved by GRAVITY, a second-generation Very Large Telescope Interferometer (VLTI) instrument (GRAVITY Collaboration 2018, 2020a, 2021b). GRAVITY has greatly improved the sensitivity of earlier efforts and has been able to combine all four of the 8 m Unit Telescope (UT) beams to yield six simultaneous baselines (GRAVITY Collaboration 2017). With a few hours of on-source exposure, GRAVITY measures the differential phase signal of a broad emission line in the near-infrared (NIR) K band, which reflects the offsets of the photocenters from the center of the continuum emission in each wavelength channel (Petrov et al. 2001; Marconi et al. 2003). The BLR size is then inferred from the differential phase data by fitting a dynamical BLR model such as the widely used model of Pancoast et al. (2014a) . The GRAVITY-measured BLR size and BH mass agree well with RM measurements (GRAVITY Collaboration 2021a,b).

GRAVITY can also resolve the size of the NIR continuum emission of the AGN, which comes from the thermal radiation of hot dust that reprocesses the UV/optical continuum from the accretion disk (e.g., Rees et al. 1969; Barvainis 1987). Spatial sizes of the dust-continuum emission can be measured by both continuum RM (e.g., Clavel et al. 1989; Baribaud et al. 1992; Glass 1992; Sitko et al. 1993; Minezaki et al. 2004, 2019; Suganuma et al. 2006; Koshida et al. 2014; Pozo Nuñez et al. 2014, 2015; Mandal et al. 2018, 2021a,b; Sobrino Figaredo et al. 2020) and optical/NIR interferometry (OI; Swain et al. 2003; Wittkowski et al. 2004; Kishimoto et al. 2009, 2011; GRAVITY Collaboration 2020b; Leftley et al. 2021). Similar to the BLR size, the dust-continuum size also scales with the AGN luminosity  $\propto L^{0.5}$  (Suganuma et al. 2006; Kishimoto et al. 2011; Koshida et al. 2014; Minezaki et al. 2019; GRAVITY Collaboration 2020b). This relation is expected if the dust temperature and the inner radius of the dust distribution are determined by radiation equilibrium and dust sublimation, respectively (Barvainis 1987; Kishimoto et al. 2007). The dust-continuum RM radius is a factor of four or five larger than the BLR radius (Koshida et al. 2014) and is consistent with BLR models that place hot dust on the outskirts of the BLR (e.g., Wang et al. 2017; Baskin & Laor 2018). Moreover, RMmeasured dust-continuum sizes are systematically smaller than those measured from OI, likely because the RM size is weighted by the time lag over the emitting region, while the OI size is weighted by the intensity of hot dust emission (Koshida et al. 2014; Kishimoto et al. 2011; GRAVITY Collaboration 2020b).

GRAVITY can observe the dust continuum independently of the full spectroastrometric measurements and has demonstrated excellent efficiency (e.g., ≤1 h per source; GRAVITY Collaboration 2020b and in prep.). Establishing a link between the BLR and dust-continuum size will enable BH mass estimations from these more accessible dust-continuum observations. In this work, we investigate the correlation between BLR and dust-continuum size in the context of estimating the BH mass. The four methods discussed in this paper are

1. The first method is reverberation mapping of the broad emission line, where a sequence of measurements over months or years, yielding the time delay for variations in the broad-line emission, leads to an estimate  $R_{\rm BLR}$ ; and hence, via Eq. (1), to the BH mass (Peterson 2014). This method has enabled empirical calibration of a sample-averaged virial factor  $\langle f \rangle$ . More recently, the velocity -resolved RM data have been shown to be able to constrain a BLR dynamical model and enable the estimation of f for individual sources (e.g., Pancoast et al. 2014a,b).

- 2. The single-epoch method is the second method. Here,  $R_{\rm BLR}$  is estimated from a single measurement of the AGN luminosity via the relation between these quantities (Shen 2013; Dalla Bontà et al. 2020). This method relies on Eq. (1) and on the virial factor calibrated via RM.
- 3. Measurements of the continuum size measurements constitute the third method, which we introduce in this paper.  $R_{\rm BLR}$  is estimated from an interferometric measurement of  $R_{\rm d}$ . Like the single-epoch method, this also relies on Eq. (1) and on a precalibration of the virial factor.
- 4. The fourth method is spectrally resolved differential phase measurements of the broad-line emission. Using the interferometric data as constraints on a dynamical BLR model, we can derive the BH mass, and hence also infer the value of the virial factor for individual sources that is independent of RM (GRAVITY Collaboration 2020a).

We show that the H $\beta$  BLR size scales tightly with the dust-continuum size, which allows us to estimate the BH mass from the dust-continuum size with an uncertainty similar to the RM BLR method. We discuss the prospects of this method for BH mass estimations in the low-redshift Universe, especially with the upgrade of GRAVITY in Sect. 5. This work adopts the following parameters for a  $\Lambda$ CDM cosmology:  $\Omega_{\rm m}=0.308$ ,  $\Omega_{\Lambda}=0.692$ , and  $H_0=67.8\,{\rm km\,s^{-1}}$  Mpc<sup>-1</sup> (Planck Collaboration XIII 2016).

## 2. Samples

#### 2.1. Dust-continuum measurements

We collect type 1 AGNs with dust-continuum sizes measured by RM and/or OI in Table 1. The dust-continuum sizes based on K-band RM observations were mainly measured by Koshida et al. (2014). Minezaki et al. (2019) summarized the results of Koshida et al. (2014) in their Table 6, using the power index  $\alpha = 0.1$  to remove the NIR emission from the accretion disk (i.e.,  $f_{\nu} \propto \nu^{\alpha}$ ) to be consistent with their primary results. The assumption of the power index may introduce a ≤10% difference in the time lag, which is typically not significant compared to the measurement uncertainty (Koshida et al. 2014; Minezaki et al. 2019). We therefore adopted the time lags from Minezaki et al. (2019) whenever available. The K-band time lag probes the dust emission size at shorter wavelength for higher-redshift sources, therefore we preferred to exclude AGNs much higher than  $z \approx 0.2$  (see also Sect. 3.3). Minezaki et al. (2019) also reported K-band continuum RM measurements for a sample of quasars at  $z \approx 0.1$ –0.6, most of which do not have H $\beta$  RM measurements. We only included three quasars from this sample, PG 0844+349, PG 0953+414, and PG 1613+658, because they have H $\beta$  RM measurements and are valuable for studying the relation of the dust continuum and BLR sizes. K-band RM measurements of the other targets, that is, 3C 120 (Ramolla et al. 2018) and H 0507+164 (Mandal et al. 2018), were collected from individual papers.

We also find 23 AGNs whose dust-continuum sizes were measured by OI, which consist of Keck (Kishimoto et al. 2009, 2011) and recent VLTI/GRAVITY observations (GRAVITY Collaboration 2020b and in prep.). Kishimoto et al. measured the dust-continuum size by fitting squared visibility amplitudes ( $V^2$ ) with a thin-ring model. They corrected for the influence of the accretion disk assuming a point source contribution to the visibilities. GRAVITY Collaboration (2020b) measured the dust-continuum size by fitting a Gaussian model to the  $V^2$ . They converted the Gaussian FWHM into the

**Table 1.** Physical properties of AGNs with dust continuum size measurements.

Name (1)	Redshift (2)	R <sub>d</sub> (RM) (ld) (3)	Ref. (4)	R <sub>d</sub> (OI) (ld) (5)	Ref.	R <sub>BLR</sub> (ld) (7)	FWHM (km s <sup>-1</sup> ) (8)	$\log \lambda L_{\lambda}(5100 \text{Å})$ $(\text{erg s}^{-1})$ $(9)$	Ref. (10)	$\log M_{\rm BH} $ $(M_{\odot})$ $(11)$	$\log \lambda_{\rm Edd}$ (12)
Mrk 335	0.0258	$167.5 \pm 6.0$	1	185 ± 49	2	$14.0 \pm 4.0$	1707 ± 79	43.8	3	$6.90 \pm 0.13$	-0.29
UGC 545	0.0612	107.5 ± 0.0		$707 \pm 77$	4	$37.2 \pm 4.7$	$1131 \pm 37$	44.5	5	$6.97 \pm 0.06$	0.39
Mrk 590 (a),(b)	0.0264	$33.5 \pm 4.2$	1			$25.6 \pm 5.9$	$2716 \pm 202$	43.5	3	$7.57 \pm 0.00$	-1.21
3C 120	0.0330	$94.4 \pm 5.5$	6	$379 \pm 85$	2	$26.2 \pm 7.7$	$2472 \pm 729$	44.0	3	$7.49 \pm 0.12$	-0.64
H0507+164	0.0179	$35 \pm 11$	7			$3.0 \pm 1.2$	$4062 \pm 247$	42.6	8	$6.99 \pm 0.18$	-1.57
Akn 120	0.0327	$138 \pm 18$	1	$387 \pm 77$	4	$39.5 \pm 8.2$	$6077 \pm 147$	43.9	3	$8.45 \pm 0.09$	-1.73
MCG+08-11-011	0.0205	$72.7 \pm 1.6$	1			$15.7 \pm 0.5$	$4139 \pm 207$	43.3	3	$7.72 \pm 0.05$	-1.54
Mrk 6 (a)	0.0205			$214 \pm 60$	9	$18.5 \pm 2.5$	$5457 \pm 16$	43.6	10	$8.03 \pm 0.06$	-1.55
Mrk 79	0.0133	$67.7 \pm 4.8$	1	214 ± 00		$15.6 \pm 5.0$	$4793 \pm 145$	43.7	3	$7.84 \pm 0.14$	-1.31
PG 0844+349	0.0222	$99 \pm 11$	1			$32.3 \pm 13.6$	$2694 \pm 58$	44.2	3	$7.64 \pm 0.14$ $7.66 \pm 0.18$	-0.59
Mrk 110	0.0353	$116.6 \pm 6.3$	1	•••	• • • •	$25.6 \pm 8.1$	$1634 \pm 83$	43.7	3	$7.00 \pm 0.18$ $7.13 \pm 0.14$	-0.59 -0.61
PG 0953+414	0.0333	$566 \pm 44$	1	•••	• • • •	$150.1 \pm 22.1$	$3071 \pm 27$	45.2	3	$8.44 \pm 0.06$	-0.01 -0.40
NGC 3227	0.2341	$14.37 \pm 0.70$	1	$45.0 \pm 7.2$	 4	$3.8 \pm 0.8$	$30/1 \pm 2/$ $4112 \pm 206$	42.2	3	$7.10 \pm 0.10$	-0.40 -2.00
NGC 3516 <sup>(a)</sup>	0.0038								3		-2.00 $-2.18$
NGC 3783	0.0088	$72.7 \pm 4.6$ $76.3 \pm 14.1$	1 11	131 ± 20	2	$11.7 \pm 1.3$ $9.6 \pm 0.7$	$5384 \pm 269$ $4486 \pm 35$	42.8 43.0	12	$7.82 \pm 0.06$	-2.18 -1.70
NGC 3783 NGC 4051	0.0097								3	$7.58 \pm 0.03$	
		$16.30 \pm 0.57$	1	$38.1 \pm 6.0$ $44.1 \pm 8.3$ (c)	13 9	$2.1 \pm 0.8$	$1076 \pm 277$	41.9	3	$5.68 \pm 0.28$	-0.92
NGC 4151 <sup>(a)</sup>	0.0033	$46.11 \pm 0.44$	1			$6.6 \pm 1.0$	$6371 \pm 150$	42.1		$7.72 \pm 0.07$	-2.77
3C 273	0.1583	$409 \pm 41$	14	$675 \pm 126$	2	$146.8 \pm 10.2$	$3314 \pm 59$	45.9	3	$8.50 \pm 0.03$	0.28
NGC 4593	0.0083	$41.82 \pm 0.90$	1	$54.8 \pm 8.8$	4	$4.0 \pm 0.8$	$5142 \pm 572$	42.6	3	$7.31 \pm 0.13$	-1.84
MCG-6-30-15	0.0078	$19.6 \pm 4.9$	15	• • •	• • • •	$5.7 \pm 1.8$	$1947 \pm 58$	41.6	3	$6.63 \pm 0.14$	-2.13
NGC 5548	0.0172	$61.21 \pm 0.30$	1	• • •	• • • •	$13.9 \pm 8.7$	$7256 \pm 2203$	43.3	3	$8.15 \pm 0.38$	-2.00
Mrk 817	0.0313	$92.6 \pm 8.9$	1	• • •	• • • •	$19.9 \pm 8.3$	$5348 \pm 536$	43.7	3	$8.05 \pm 0.20$	-1.45
PG 1613+658	0.1211	$334 \pm 40$	1	• • • •	• • • •	$40.1 \pm 15.1$	$9074 \pm 103$	44.8	3	$8.81 \pm 0.16$	-1.19
Z 229-15	0.0279	$20.4 \pm 5.8$	16			$3.9 \pm 0.8$	$3350 \pm 72$	42.9	17	$6.93 \pm 0.09$	-1.18
Mrk 509	0.0344	$121.3 \pm 1.6$	1	$297 \pm 31$	2	$79.6 \pm 5.8$	$3015 \pm 2$	44.2	3	$8.15 \pm 0.03$	-1.11
NGC 7469	0.0163	$85.29 \pm 0.43$	1		• • •	$10.8 \pm 2.4$	$4369 \pm 6$	43.5	3	$7.60 \pm 0.10$	-1.24
NGC 1365 (a)	0.0055	• • •		$38.1 \pm 4.8$	2	• • •	$1586 \pm 465$	41.9	2 <sup>(f)</sup> ,18		
IRAS 03450+0055	0.0315	$157.4 \pm 5.9$	1				$3098 \pm 55$	43.9	1,19	• • •	
IRAS 09149-6206 (d)	0.0573			$482 \pm 49$	2		$4281 \pm 121$	45.0	20,21	$8.06 \pm 0.25$	-0.26
Mrk 1239	0.0199			$189 \pm 30$	4		$830 \pm 10$	44.5	22 <sup>(f)</sup>		
WPVS 48	0.0370	$70.8 \pm 4.6$	23				$1890 \pm 60$	43.6	24		
Mrk 744	0.0091	$19.9 \pm 2.2$	1				$5616 \pm 129$	41.8	1,21 <sup>(g)</sup>		
HE 1029-1401	0.0858			$880 \pm 133$	4		$5684 \pm 284$	44.6	21		
GQ Com	0.1650	$210 \pm 40$	25				$5036 \pm 252$	44.6	26		
Mrk 231	0.0422			$393 \pm 83$	13		$3130 \pm 156$	45.0	2 <sup>(f)</sup> ,27		
ESO 323-G77	0.0150			$100.0 \pm 4.8$	28		$2635 \pm 132$	43.1	21		
IRAS 13349+2438	0.1076			$1096 \pm 71$	13		$1796 \pm 90$	45.0	29		
IC 4329A	0.0161			$178 \pm 10$	4		$6472 \pm 324$	43.2	21		
PGC 50427 (e)	0.0235	$46.7 \pm 2.2$	30				$3036 \pm 74$	43.1	30	$7.34 \pm 0.04$	-1.42
PDS 456	0.1840			$1599 \pm 213$	2		$3974 \pm 764$	46.3	31		
PGC 89171	0.0270			$303 \pm 36$	4		$2644 \pm 132$	43.9	21		
NGC 7603	0.0288			$332 \pm 66$	4		$6350 \pm 318$	44.4	21		

Notes. <sup>(a)</sup>This target is discussed as a changing-look quasar in the literature. <sup>(b)</sup>Mrk 590 is a changing look AGN displaying strong variability over the time of BLR and dust continuum observations (Denney et al. 2014). We do not include it in our statistical analysis. <sup>(c)</sup>The continuum radius of NGC 4151 reported by Kishimoto et al. (2011) is statistically consistent with the recent measurement from Kishimoto et al. (2022). We prefer the early measurements because it is close to the RM measurement. <sup>(d)</sup>The BLR of IRAS 09149–6206 was resolved by GRAVITY and the BH mass is derived by GRAVITY Collaboration (2020a). The  $\lambda L_{\lambda}$ (5100 Å) and FWHM of H $\beta$  are from the BASS catalog (Koss et al. 2017). <sup>(e)</sup>The BH mass of PGC 50427 was measured by RM of the H $\alpha$  line (Pozo Nuñez et al. 2015). We quote the  $\lambda L_{\lambda}$ (5100 Å) from Probst & Kollatschny (2020) observed close in time to H $\alpha$  RM. We measure the FWHM of H $\beta$  line from the 6dF spectrum (Jones et al. 2009). <sup>(f)</sup>We converted the bolometric luminosity to  $\lambda L_{\lambda}$ (5100 Å) using Eq. (A.2) of GRAVITY Collaboration (2020b). <sup>(g)</sup>H $\beta$  FWHM is converted from H $\alpha$  FWHM assuming FWHM<sub>H $\beta$ </sub>/FWHM<sub>H $\alpha$ </sub> = 1.17 citepGreene2005. Column (1): Target name. Column (2): Redshift from NASA/IPAC Extragalactic Database (NED). Column (3): Dust continuum radius based on RM measurement. Column (4): Reference of  $R_d$  (RM). Column (5): Dust continuum radius based on OI measurement. Column (6): Reference of  $R_d$  (OI). Column (7): BLR radius based on H $\beta$  time lag. Column (8): H $\beta$  FWHM. Column (9): AGN optical luminosity at 5100 Å. Column (10): References of  $R_{BLR}$ , FWHM, and  $\lambda L_{\lambda}$ (5100Å). Column (11): BH mass derived from  $R_{BLR}$  and FWHM from Cols. (7) and (8) assuming the virial factor f = 1. Column (12): Eddington ratio derived from  $\lambda L_{\lambda}$ (5100 Å) and BH mass from Cols. (9) and (11) with the bolometric correction factor 9 (Peterson et al. 2004).

References. (1) Minezaki et al. (2019), (2) GRAVITY Collaboration (2020b), (3) Du & Wang (2019), (4) GRAVITY Collaboration (in prep.), (5) Huang et al. (2019), (6) Ramolla et al. (2018), (7) Mandal et al. (2018), (8) Stalin et al. (2011), (9) Kishimoto et al. (2011), (10) Du et al. (2018), (11) Lira et al. (2011), (12) Bentz et al. (2021), (13) Kishimoto et al. (2009), (14) Sobrino Figaredo et al. (2020), (15) Lira et al. (2015), (16) Mandal et al. (2021a), (17) Barth et al. (2011), (18) Onori et al. (2017), (19) Rashed & Eckart (2015), (20) GRAVITY Collaboration (2020a), (21) Koss et al. (2017), (22) Pan et al. (2021), (23) Pozo Nuñez et al. (2014), (24) Probst & Kollatschny (2020), (25) Sitko et al. (1993), (26) Shangguan et al. (2018), (27) Zheng et al. (2002), (28) Leftley et al. (2021), (29) Dong et al. (2018), (30) Pozo Nuñez et al. (2015), (31) Nardini et al. (2015).

thin-ring radius and corrected the radius assuming a 20% contribution of the coherent flux from the accretion disk. Recent GRAVITY observations measured the dust-continuum size of 7 AGNs with an observation time of ≲one hour per source (GRAVITY Collaboration, in prep.). We follow the method of GRAVITY Collaboration (2020b) to measure their continuum size. To estimate the uncertainty, we summed the statistical uncertainty of the size measurements of individual exposures in quadrature and a 10% systematic uncertainty (GRAVITY Collaboration 2020b and in prep.).

#### 2.2. BLR measurements

The BLR size can be probed by different broad emission lines. The H $\beta$  line has been the most extensively used in RM campaigns of low-z AGNs (e.g., Bentz & Katz 2015). GRAVITY spectroastrometric observations probe the BLR with  $Pa\alpha$  and Bry (GRAVITY Collaboration 2018, 2020a, 2021b). Different broad lines of a BLR may show a different size due to the photoionization conditions and optical depth (Korista & Goad 2004). We only studied the relation of the dust-continuum radius and H $\beta$  BLR radius from the RM time lag for simplicity. Future GRAVITY observations measuring the BLR and dust continuum simultaneously in K band will be powerful enough to investigate their relation (see Sect. 5). We collected the H $\beta$  BLR radii of most targets, together with their optical luminosities at 5100 Å and H $\beta$  line FWHMs from Table 1 of Du & Wang (2019)<sup>1</sup>. Du & Wang (2019) averaged the quantities when more than one measurement was available. We only found a few additional AGNs from the other references (see Table 1). We adjusted the  $\lambda L_{\lambda}(5100\,\text{Å})$  to our cosmology when necessary, unless the distances of some nearby AGNs are explicitly specified in the references.

#### 2.3. AGN variability

We emphasize that the BLR and dust-continuum sizes are usually measured in different epochs. While the BLR RM campaigns of many targets conducted from 2000–2010 coincide with dust-continuum RM campaigns (Koshida et al. 2014; Minezaki et al. 2019), the time difference between BLR and dust measurements for some targets can be over a decade. For example, we adopted the BLR RM of NGC 3783 measured in 2020 (Bentz et al. 2021), while its dust-continuum RM was measured in about 2009 (Lira et al. 2011). The early BLR RM measurements of NGC 3783 (Onken & Peterson 2002) yielded a BLR radius and  $\lambda L_{\lambda}$ (5100 Å) quite close to the recent measurements. We therefore preferred to adopt the new measurements for simplicity. The asynchronous effect contributes to the scatter of the size correlation (see the discussion in Sect. 3).

Targets with substantial variability may show large scatter in the  $R_{\rm BLR}$ – $R_{\rm d}$  relation. We identified so-called changing-look AGNs in our sample from the literature and discuss them in the following. In the end, we are convinced that only Mrk 590 cannot be included in our analysis. Mrk 590 transformed from a classical type 1 AGN to type 1.9–2, as its continuum luminosity decreased by 100 over the past four decades (Denney et al. 2014). The lack of evidence of intrinsic absorption indicates that changes in continuum and emission lines are due to the decline of the BH accretion rate instead of obscuration along the line of sight. The BLR of Mrk 590 was monitored through the H $\beta$  line from 1990 to 1996 (Peterson et al. 1998) and with

 $H\alpha$  in 2018 (Mandal et al. 2021b). The BLR size of Mrk 590, about 25 ld, does not change significantly in the bright and faint states. The dust-continuum RM campaign was conducted from 2003 to 2007 (Koshida et al. 2014) during the rapid decline of the AGN luminosity in Mrk 590. Kokubo & Minezaki (2020) found that the dust-continuum size of Mrk 590 is quite small, only ~33 ld, reflecting the rapid replenishment of the dust in the innermost region of the dusty interstellar medium. We excluded Mrk 590 from our statistics to avoid the complicated physics of this target. Other changing-look AGNs are included in our sample, for instance, Mrk 6 and NGC 4151 (flagged in Table 1). They change either from type 1 to type 2 or vice versa (see Marin et al. 2019; Senarath et al. 2021 and references therein). However, the BLR and continuum were measured when they stayed the same type, therefore we include them in our analysis. Moreover, some changing-look AGNs flagged in our sample are likely caused by temporary changes in the line-of-sight obscuration (e.g., Goodrich 1989; Shapovalova & Popović 2019). This mechanism does not relate to any intrinsic change in the AGN properties, therefore it will not affect the  $R_{\rm BLR}$ - $R_{\rm d}$  relation that we are interested in for this work. Nevertheless, our results stay the same when we exclude all the changing-look AGNs. Clavel et al. (1989) published their K-band RM measurement of Fairall 9 while its UV continuum flux was dropping by a factor of ~30. However, no H $\beta$  RM measurement before it changed to the faint state is available. The extreme variability, from type 1 to almost type 2 (Kollatschny & Fricke 1985; Lub & de Ruiter 1992), prevents a simple choice of  $\lambda L_{\lambda}(5100 \,\text{Å})$  and H $\beta$  FWHM for our analysis. Therefore, we chose to exclude Fairall 9 from this work.

## Scaling relations of BLR and dust-continuum size

Figure 1 displays our sample. The dust *R*–*L* relations measured by both RM and OI are systematically above the BLR *R*–*L* relation. Moreover, the continuum size measured by OI is above that of RM. The R-L relations of dust RM and OI measurements have been discussed in many previous works (e.g., Suganuma et al. 2006; Kishimoto et al. 2009, 2011; Koshida et al. 2014; Minezaki et al. 2019; GRAVITY Collaboration 2020b). One common explanation is that the RM-measured time lag is weighted by the amplitude of flux variations, which is expected to originate most strongly from the inner boundary of the hot dust; on the other hand, OI-measured sizes are mainly flux-weighted and are therefore elevated by contributions of lower-temperature dust at larger radii (Kishimoto et al. 2009, 2011). Another slightly different explanation assumes that the dust structure has a bowl shape (Kawaguchi & Mori 2010): We mainly observe the foreground side at a low inclination angle for type 1 AGNs, and dust at larger radii is also closer to the observer, so that the projected size increases more significantly than their RM time lag toward larger radii (Pozo Nuñez et al. 2014; Sobrino Figaredo et al. 2020). A more detailed discussion of BLR and dust-structure models is beyond the scope of this paper. Throughout the paper, we use OI and RM to refer to the dust-continuum measurements from these two different methods unless otherwise clarified.

Previous works studying both RM and OI observations have indicated that the slope of the dust-continuum R-L relation is shallower than  $\propto L^{0.5}$ . The slopes in our current RM and OI samples are both about 0.4, consistent with previous works. We leave a more detailed discussion of the R-L relation for a separate

<sup>&</sup>lt;sup>1</sup> Similar data are also collected in Dalla Bontà et al. (2020).

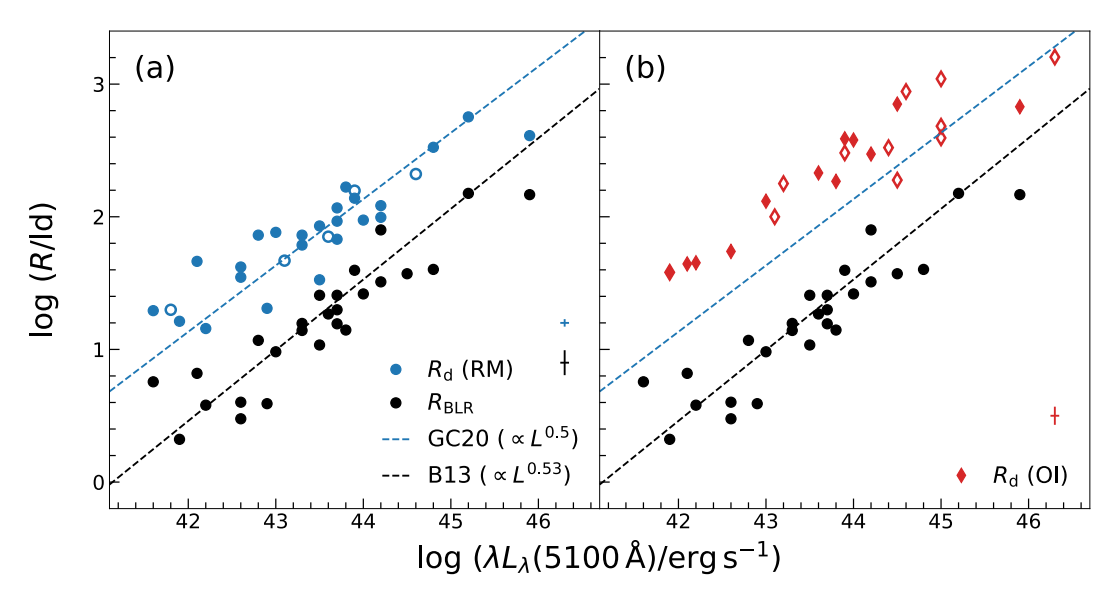


**Fig. 1.** Size–luminosity relations of the dust continuum measured by (*a*) RM (blue circles) and (*b*) OI (red diamonds) are systematically above that of the BLR (black circles; same in both panels). The open-colored circles indicate sources without BLR measurements. The dashed lines in both panels are based on RM-measured *R*–*L* relations of the dust continuum (blue; GRAVITY Collaboration 2020b) and the BLR (black; Bentz et al. 2013). The typical uncertainties are shown on the lower right of each panel.

paper (GRAVITY Collaboration et al., in prep.). In summary, previous RM studies provided various explanations of the shallower slope relating to the dust structure, dust response to the accretion disk emission, and its putative effect on the observed optical luminosity (e.g., Minezaki et al. 2019; Sobrino Figaredo et al. 2020). Based on the OI measurements, GRAVITY Collaboration (2020b) suspected that the continuum emission of the accretion disk may bias the OI size measurement for the most luminous sources.

Likewise, recent RM BLR measurements (Du et al. 2015; Grier et al. 2017) also reported targets with  $R_{\rm BLR}$  significantly lower than the canonical BLR R–L relation (e.g., Bentz et al. 2013). Some works reported that the deviation closely correlates with the accretion rate of the BH (Du et al. 2015; Du & Wang 2019; Martínez-Aldama et al. 2019; Dalla Bontà et al. 2020), while the physical driver remained unclear in some other works (Grier et al. 2017; Fonseca Alvarez et al. 2020). The physical explanation of the deviation of BLR and dust-continuum R–L relations is beyond the scope of the current paper. As discussed in the following sections, we find tight relations between  $R_{\rm BLR}$  and  $R_{\rm d}$  that are close to linear, reflecting a simple link between the two physical structures.

## 3.1. Statistical analysis

We find strong correlations between BLR and dust-continuum sizes, as shown in Fig. 2. We fit the relations for RM- and OI-measured  $R_d$  separately as they show systematic differences. We fit the data with a power-law relation,

$$\log (R_{\rm BLR}/{\rm Id}) = \alpha + \beta \log (R_{\rm d}/R_{\rm d,0}), \tag{2}$$

where  $\alpha$  and  $\beta$  are the intercept and the slope, and  $R_{\rm d,0}$  is a pivot point fixed close to the median of  $R_{\rm d}$  of the data to reduce the degeneracy of  $\alpha$  and  $\beta$ . We adopted the Bayesian Markov chain Monte Carlo (MCMC) approach to fit the data. The likelihood is

$$\ln \mathcal{L} = -\frac{1}{2} \Sigma_i \left( \ln(2\pi\sigma_i^2) + \frac{(y_i - m_i)^2}{\sigma_i^2} \right), \tag{3}$$

where  $y_i$  is  $\log R_{\rm BLR}$  data,  $m_i$  is the model value based on  $\log R_{\rm d}$  and Eq. (2), and  $\sigma_i^2 = (\beta \, \sigma_{x,i})^2 + \sigma_{y,i}^2 + \epsilon^2$  includes the measurement uncertainties of the dust-continuum  $(\sigma_{x,i})$  and BLR  $(\sigma_{y,i})$  radius as well as the intrinsic scatter  $(\epsilon)$ . We adopted uniform priors of the parameters that are wide enough and sample the posterior with the widely used Python package of MCMC, emcee (Foreman-Mackey et al. 2013). We used 32 walkers and 5000 steps; the first 500 steps were discarded as burn-in steps. The fitting converged well.

The best-fit relations are very close to linear (throughout the paper, 'linear' refers to  $\beta=1$ ) when we allow the slope to be free, as shown in Figure 2a. Therefore, we also fit the data with the slope fixed to unity (Fig. 2b). The best-fit results are listed in Table 2. For simplicity, we take the  $\beta$ -fixed fitting results in the following discussion and derive the BLR radius and BH mass with  $R_{\rm d}$  in Sect. 4. Because of the current uncertainties, it does not affect these results whether we adopt the relations with  $\beta$  free or fixed.

The dust-continuum size measured from RM is about 0.7 dex (five times) larger than the BLR size, which is consistent with previous works (e.g., Koshida et al. 2014; Kokubo & Minezaki 2020). The dust-continuum size measured by OI is about 0.3 dex (two times) larger than that measured by RM, again consistent with previous studies (Kishimoto et al. 2011; Koshida et al. 2014; GRAVITY Collaboration 2020b). We do not find the slope of the  $R_{\rm BLR}-R_{\rm d}$  relation to significantly deviate from unity. However, for the relation to be linear, any departure from  $\propto L^{0.5}$  for the R-L relations of the dust continuum and the BLR must be similar. Our sample shows a more significant deviation in  $R_{\rm d}-\lambda L_{\lambda}(5100~{\rm \AA})$  than that in  $R_{\rm BLR}-\lambda L_{\lambda}(5100~{\rm \AA})$ . This difference may contribute to the scatter of the  $R_{\rm BLR}-R_{\rm d}$  relation, which we discuss in Sect. 3.3.

#### 3.2. Intrinsic scatter

The intrinsic scatter of the best-fit relations is about 0.25 dex for both RM and OI relations. The physical difference between the BLR and dust structure for individual targets may contribute to

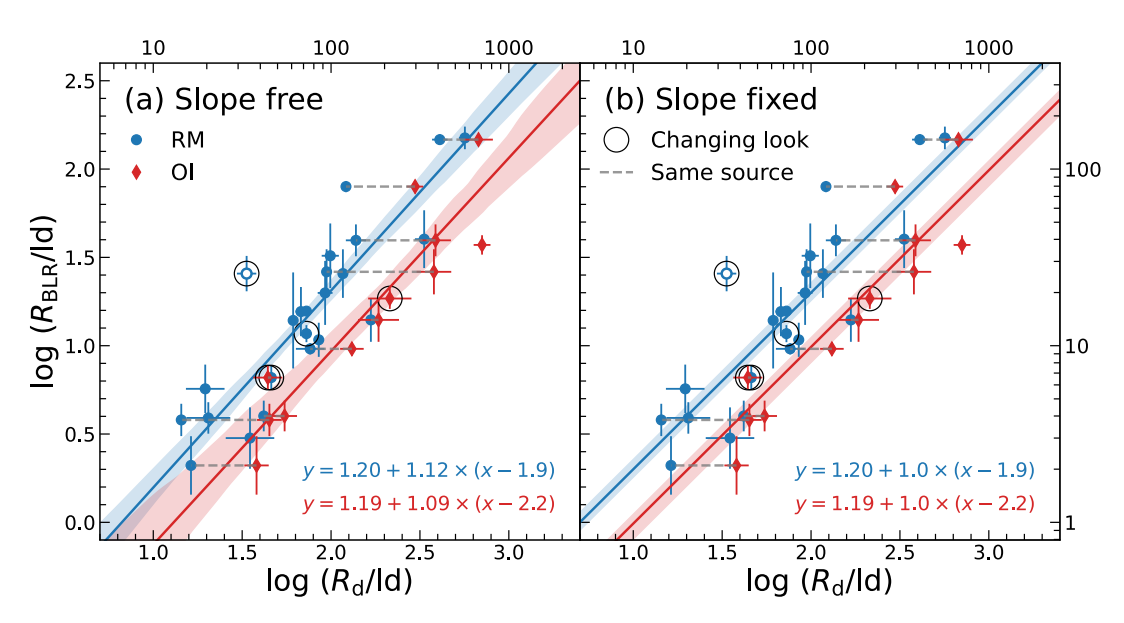


**Fig. 2.** Tight relations between the radii of the BLR and the dust continuum. The blue circles are AGNs measured by RM, and the red diamonds are the targets measured by OI. The dashed gray lines connect the same sources with both RM and OI measured  $R_{\rm d}$ . The best-fit  $R_{\rm BLR}-R_{\rm d}$  relations of RM and OI datasets (formula in the lower right corner of each panel) are shown as the blue and red lines, respectively. The black circles enclose the known changing-look AGNs. We only exclude Mrk 590, denoted as the empty blue circle, from our analysis. The linear scale is indicated on the top and right axes.

the scatter. Such a variation was observed in the mid-IR, where a large scatter of the R-L relation was observed (Burtscher et al. 2013). However, in addition to the individual BLR and dust structure difference, the uncertainty of the bolometric luminosity of an AGN for the R-L relation is another primary source of the scatter. Studying the BLR and dust structure with the  $R_{\rm BLR}-R_{\rm d}$  relation allows us to avoid the uncertain bolometric luminosity. However, AGN variability still likely introduces considerable intrinsic scatter because the BLR and dust-continuum sizes are not measured in a state in which they reflect the same AGN bolometric luminosity.

As described in Sect. 2.3, most of the dust continuum RM measurements were made between 2001 and 2008, while the OI measurements were conducted in about 2009-2010 (Keck interferometry) and 2018-2022 (GRAVITY). The BLR measurements were conducted from the 1980s until recent years. NGC 5548 is one of the best targets to investigate the variability: Du & Wang (2019) collected 18 epochs of its BLR RM measurements from 1989 to 2015, and the BLR radius (time lag) varies from 4.21d to 26.51d with a standard deviation of 0.24 dex. Mrk 335 and Mrk 817 also have 4 epochs of BLR measurements in >10 years, and their BLR radii changes are  $\gtrsim 0.3$  dex. For the dust continuum, Koshida et al. (2014) reported 6 epochs of dustcontinuum RM measurements for NGC 5548 from 2001 to 2007; the RMS of the dust-continuum radius is about 0.1 dex. Other AGNs, NGC 3227, NGC 4051, and NGC 4151, with  $\geq$ 4 epochs of dust RM measurements, also show similar ~0.1 dex RMS variation. NGC 3783 was observed from 1974-1990 (Glass 1992) and later in 2006–2009 (Lira et al. 2011); the measured K-band time lags are consistent within their uncertainties. It is not surprising that the dust-continuum size shows less variability: the dust reradiation effectively averages the variability of the central engine on a longer timescale, while the RM technique measures the averaged size over the monitoring period.

Because the BLR size variation of the AGNs with multiple measurements always reaches  $\gtrsim 0.2$  dex, we conclude that the observed 0.25 dex intrinsic scatter of the  $R_{\rm BLR}$ – $R_{\rm d}$  relations

**Table 2.** Best-fit parameters of Eq. (2).

Relation	α	β	$\epsilon$	$\log (R_{d,0}/\mathrm{ld})$
RM (free)	$1.20^{+0.05}_{-0.05}$	$1.12^{+0.13}_{-0.13}$	$0.21^{+0.05}_{-0.04}$	1.9
OI (free)	$1.19^{+0.08}_{-0.08}$	$1.10^{+0.18}_{-0.18}$	$0.25^{+0.08}_{-0.06}$	2.2
RM (fixed)	$1.20^{+0.05}_{-0.05}$	1	$0.21^{+0.04}_{-0.04}$	1.9
OI (fixed)	$1.19^{+0.08}_{-0.08}$	1	$0.24^{+0.07}_{-0.05}$	2.2

**Notes.** We fit the  $R_{\rm BLR}-R_{\rm d}$  relation for AGNs with  $R_{\rm d}$  measured by RM and OI, respectively.  $\alpha$ ,  $\beta$ , and  $\epsilon$  are the intercept, slope, and intrinsic scatter of a linear relation.  $R_{\rm d,0}$  is the pivot point fixed in the fitting. The first two rows provides the best-fit parameters with  $\beta$  free, while the last two rows are results with  $\beta$  fixed to unity. OI-measured  $R_{\rm d}$  is about 0.3 dex larger than that measured by the RM.

can be explained by the time variation of the BLR and dust-continuum sizes, while the physical difference between the BLR and dust structures of individual targets also plays a role. Future simultaneous measurements of BLR and dust-continuum sizes have the potential to reveal a tighter  $R_{\rm BLR}$ – $R_{\rm d}$  relation, while the related caveats are discussed in Sect. 4.3.

#### 3.3. Higher-order correlations

We investigated whether the scatter of the  $R_{\rm BLR}-R_{\rm d}$  relation correlates with the physical properties of the AGN. Because the  $R_{\rm BLR}-R_{\rm d}$  relations are remarkably close to linear (Sect. 3.1), we studied the dependence of the ratio,  $R_{\rm BLR}/R_{\rm d}$ , on the other physical parameters of the AGN. We calculated Spearman's rank correlation coefficients to test the significance of the correlations. We perturbed  $R_{\rm BLR}/R_{\rm d}$  500 times with the measurement uncertainties of  $R_{\rm BLR}$  and  $R_{\rm d}$  to calculate the p-value distribution. The resulting p-values do not support any significant correlations (i.e., p > 0.05). We find that the conclusions do not change when we study the deviation of the  $R_{\rm BLR}-R_{\rm d}$  relations from the best-fit results with  $\beta$  free.

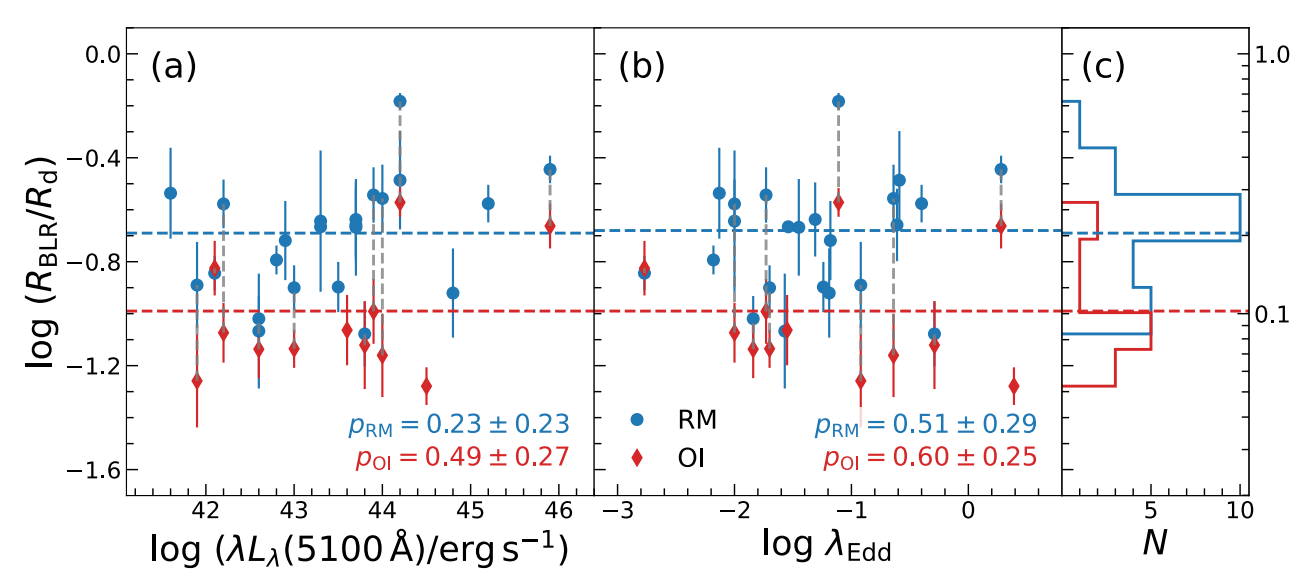


Fig. 3. Ratio of BLR and dust continuum sizes as a function of (a) the AGN luminosity and (b) the Eddington ratio. The p-values of Spearman's rank correlation coefficient are reported in the lower right corner of each panel for RM- and OI-measured samples. The notations are the same as in Fig. 2. The error bars are the quadrature sum of the uncertainties of  $R_{\rm BLR}$  and  $R_{\rm d}$ . Panel c displays the histograms of the ratios. The dashed lines indicate the averaged  $R_{\rm BLR}/R_{\rm d}$  based on the fitting of the  $R_{\rm BLR}-R_{\rm d}$  relations with  $\beta$  fixed to unity (see also Eq. (4)).  $R_{\rm BLR}/R_{\rm d}$  does not show a statistically significant correlation with the  $\lambda L_{\lambda}(5100\,\text{Å})$  or the Eddington ratio. The linear scale of  $R_{\rm BLR}/R_{\rm d}$  is indicated on the right.

We first investigated  $R_{\rm BLR}/R_{\rm d}$  against the AGN luminosity and the Eddington ratio (Fig. 3). Although the p-values do not support significant correlations, we note that at  $\lambda L_{\lambda}(5100 \,\text{Å}) >$ , the three data points of PG 0953+414 and 3C 273 are all above the averaged values of  $R_{\rm BLR}/R_{\rm d}$ . This trend may drive the slope to values slightly higher than 1 when we fit the  $R_{\rm BLR}$ - $R_{\rm d}$  relation with the slope free. Unfortunately, our current sample has too few luminous AGNs to confirm this trend. Previous BLR RM studies have found that the Eddington ratio may drive the deviation of the R-L relation such that highly accreting AGNs display shorter time lags (e.g., Du et al. 2015). We do not find a dependence of  $R_{\rm BLR}/R_{\rm d}$  on the Eddington ratio. Nevertheless, our targets do not show significant deviation from the Bentz et al. (2013) relation either (Fig. 1). It is worth noting that Mrk 509, which displays the highest deviation of  $R_{\rm BLR}/R_{\rm d}$ , has only  $\lambda L_{\lambda}(5100 \,\text{Å}) \approx 10^{44.2} \,\text{erg s}^{-1}$  and an intermediate Eddington ratio. More observations are needed to understand the details of the  $R_{\rm BLR}$ – $R_{\rm d}$  relation.

We further investigated the dependence of  $R_{\rm BLR}/R_{\rm d}$  on  $R_{\rm d}$ ,  $R_{\rm BLR}$ , and the FWHM of H $\beta$  (Fig. 4). Again, Spearman's rank correlation coefficients do not support a significant correlation with any of the three parameters. We only find a tentative trend that all three targets, PG 0953+414, 3C 373, and Mrk 509, with  $R_{\rm BLR} \gtrsim 50\,\rm ld$  in Fig. 4b show  $R_{\rm BLR}/R_{\rm d}$  above the averaged values. This trend is similar to what is discussed above for  $\lambda L_{\lambda}(5100\,\rm \mathring{A}) > 10^{45}\,\rm erg\,s^{-1}$  AGNs, although we caution that the intrinsic scatter of the  $R_{\rm BLR}-R_{\rm d}$  relation will naturally lead to the correlation between  $R_{\rm BLR}/R_{\rm d}$  and  $R_{\rm BLR}$ .

Moreover, in our sample, AGNs with the largest radii are at  $z \gtrsim 0.1$ . Their K-band measurements probe continuum emission at a slightly shorter wavelength ( $\lesssim 2\,\mu\text{m}$ ) than the rest of the sample. The continuum size may simply be exptected to be smaller at shorter wavelengths because higher temperature dust that is closer to the central engine contributes more (e.g., Oknyansky et al. 2015). A sharp decrease in the time lag toward shorter wavelength was indeed observed for NGC 4151 (Oknyanskij et al. 1999) and GQ Com (Sitko et al. 1993). However, it is more common that the time lags of dust

emission only decrease moderately toward shorter wavelength (Oknyansky et al. 2015). A biconical dust distribution can explain this because dust with different temperatures is located on similar isodelay surfaces. Therefore, we suggest that the redshift effect is not likely to cause the observed deviation. However, it is hard to draw a firm conclusion with the limited number of measurements. More observations of AGNs with high luminosity and/or at high redshift are essential to investigate this problem further.

## 4. Estimating BH masses with dust-continuum sizes

### 4.1. BLR radius based on dust-continuum measurements

We can now use the measured dust-continuum radius to estimate the BLR radius for AGNs lacking BLR measurements. We adopted the best-fit parameters with  $\beta=1$  in Table 2 so that Eq. (2) can be written as

$$\log R_{\rm BLR} = \begin{cases} \log R_{\rm d} - 0.70 & ({\rm RM}), \\ \log R_{\rm d} - 1.01 & ({\rm OI}). \end{cases}$$
 (4)

We adopted 0.25 dex as the uncertainty of  $R_{\rm BLR}$  based on the intrinsic scatter of the  $R_{\rm BLR}$ – $R_{\rm d}$  relation. We expect the uncertainty of the  $R_{\rm BLR}$ – $R_{\rm d}$  relations to be reduced in the future with more observations of the BLR and continuum close in time and of more luminous AGNs with large BLR sizes (however, see Sect. 4.3).

In Table 3, we report the  $R_{\rm BLR}$  derived from Eq. (4) for AGNs in the lower part of Table 1. We plot these targets in Fig. 5 with their  $R_{\rm BLR}$  against  $\lambda L_{\lambda}(5100~{\rm Å})$ . The continuum-based  $R_{\rm BLR}$  follows the R-L relation of the direct BLR measurements. Similar to the results of Du & Wang (2019) and Grier et al. (2017), we find that AGNs lie more likely below the Bentz et al. (2013) relation, especially for the luminous ( $\lambda L_{\lambda}(5100~{\rm Å}) > 10^{44}~{\rm erg~s^{-1}})$  objects. Although we are still limited by the small number of objects, the distribution of our targets closely resembles

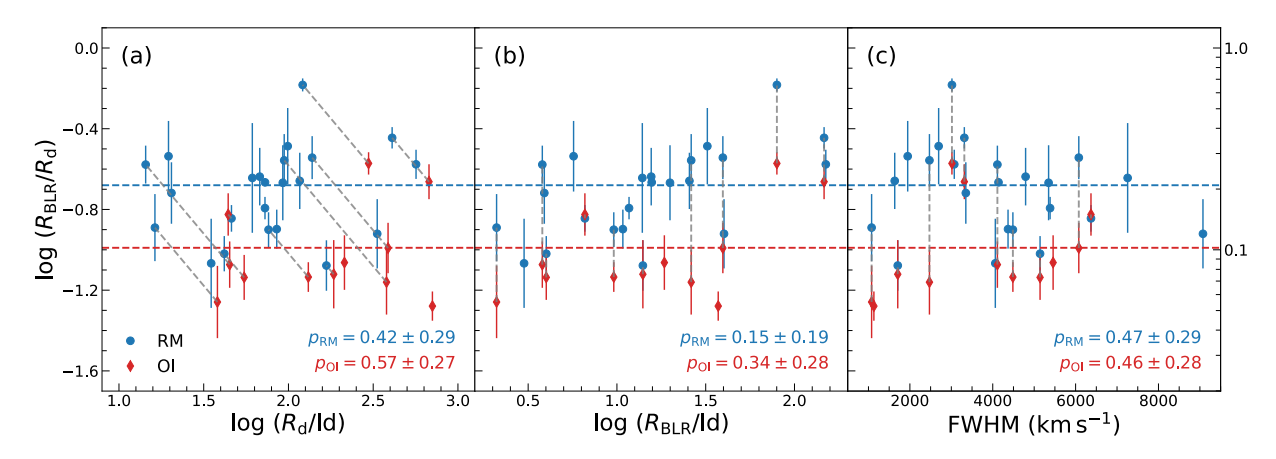


Fig. 4. Ratio of  $R_{\rm BLR}$  and  $R_{\rm d}$  as a function of (a) the continuum radius, (b) the BLR radius, and (c) the FWHM of H $\beta$  line. We do not find any statistically significant correlation. However, all of the AGNs with  $R_{\rm BLR} \gtrsim 50\,\rm ld$  show  $R_{\rm BLR}/R_{\rm d}$  above the averaged values. We discuss this tentative trend in the text. The notations are the same as in Fig. 3. The linear scale of  $R_{\rm BLR}/R_{\rm d}$  is indicated on the right.

Table 3. BH mass and Eddington ratio derived with dust continuum

Name	$\log R_{\rm BLR}$	$\log M_{\rm BH}$	$\log \lambda_{\rm Edd}$
	(ld)	$(M_{\odot})$	
(1)	(2)	(3)	(4)
NGC 1365	$0.57 \pm 0.26$	6.26	-1.51
IRAS 03450+0055	$1.50 \pm 0.25$	7.77	-1.02
IRAS 09149-6206	$1.67 \pm 0.25$	8.23	-0.37
Mrk 1239	$1.27 \pm 0.26$	6.40	0.96
WPVS 48	$1.15 \pm 0.25$	6.99	-0.54
HE 1029-1401	$1.93 \pm 0.26$	8.73	-1.28
Mrk 744	$0.60 \pm 0.25$	7.39	-2.73
GQ Com	$1.62 \pm 0.26$	8.32	-0.86
Mrk 231	$1.58 \pm 0.27$	7.87	-0.01
ESO 323-G77	$0.99 \pm 0.25$	7.12	-1.17
IRAS 13349+2438	$2.03 \pm 0.25$	7.83	0.02
IC 4329A	$1.24 \pm 0.25$	8.17	-2.10
PGC 50427	$0.97 \pm 0.25$	7.22	-1.27
PDS 456	$2.19 \pm 0.26$	8.68	0.47
PGC 89171	$1.47 \pm 0.26$	7.61	-0.85
NGC 7603	$1.51 \pm 0.26$	8.41	-1.15

**Notes.** Column (1): Target name. Column (2): BLR radius derived from  $R_d$  with Eq. (4). However, we find the difference between the results using the best-fit relations with  $\beta$  fixed and free is much smaller than the uncertainties. Column (3): BH mass derived from  $R_{\rm BLR}$  and H $\beta$  FWHM assuming the virial factor f = 1. Column (4): Eddington ratio derived from  $\lambda L_d$  (5100 Å) (Col. (9) of Table 1) and BH mass from Col. (3).

the RM-measured sample. Four targets, Mrk 1239, Mrk 231, IRAS 09149–6206, and PDS 456, show the most significant deviation from the Bentz et al. (2013) relation. As discussed in Sect. 4.2, all of them, except for IRAS 09149–6206, are at or above their Eddington luminosity. The Eddington ratio of IRAS 09149–6206 (about 0.4) is also high among the typical AGNs (e.g., the rest of the sample). Thus the large deviations from the *R*–*L* relation could be related to their high accretion rates (Du & Wang 2019).

### 4.2. BH mass

Because our continuum-based  $R_{\rm BLR}$  is fully consistent with RM-measured  $R_{\rm BLR}$ , Eq. (1) and the virial factor previously cali-

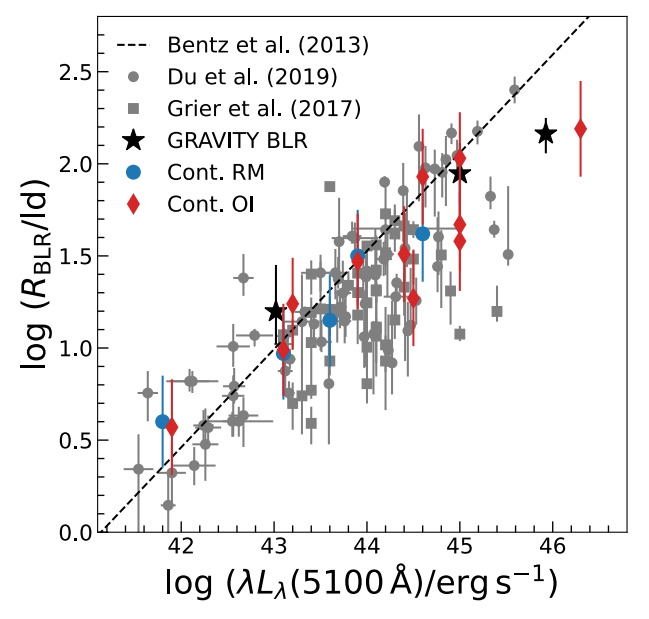


**Fig. 5.** BLR *R–L* relation of AGNs measured by the continuum-based method. The blue circles and red diamonds are based on dust radii measured by RM and OI, respectively. The black stars are three AGNs whose BLR kinematics are resolved by GRAVITY (GRAVITY Collaboration 2018, 2020a, 2021b). The gray circles and squares are BLR RM measured AGNs from Du & Wang (2019) and Grier et al. (2017), respectively. The dashed line is the best-fit *R–L* relation from Bentz et al. (2013). The continuum-based method derives the BLR radii following a similar trend of the *R–L* relation based on RM and GRAVITY BLR measurements.

brated for the RM method can be adopted to derive the BH mass. We adopted f=1 to be consistent with Du & Wang (2019). The FWHM of the H $\beta$  line can be obtained from a single-epoch spectrum (Table 1). We further calculated the Eddington ratios of these targets with the bolometric luminosities scaled from  $\lambda L_{\lambda}(5100 \text{ Å})$  by a bolometric correction factor of 9 (Peterson et al. 2004). Four AGNs, Mrk 1239, Mrk 231, IRAS 13349+2438, and PDS 456, are close to or above the Eddington accretion. Their optical spectra (see their references in Col. (10) of Table 1) commonly show narrow widths of the broad H $\beta$  lines, weak or no [OIII]  $\lambda\lambda$ 4959,5007 lines, and strong FeII features. These features strongly indicate that these targets

have high accretion rates (Boroson & Green 1992; Shen & Ho 2014 and references therein), consistent with our Eddington ratios. The BH masses of IRAS 09149–6206 and PGC 50427 are  $10^{8.06}\,M_\odot$  and  $10^{7.34}\,M_\odot$ , based on the spectroastrometry of the broad Bry line GRAVITY Collaboration (2020a) and the RM of H\$\alpha\$ line (Pozo Nu\tilde{n}ez et al. 2015), respectively. Our derived BH masses by the continuum-based method are very close (<0.2 dex) to those from the direct BLR measurements.

The primary uncertainty of the RM method in measuring the BH mass comes from the virial factor. The calibration of f typically shows ~0.4 dex intrinsic scatter (Woo et al. 2010; Ho & Kim 2014), which consists of the variation in the BLR structure of individual targets and the intrinsic scatter of the  $M_{\rm BH}$ - $\sigma_*$ relation (Gebhardt et al. 2000; Ferrarese & Merritt 2000). The sample selection and regression method may introduce a systematic difference of a factor of 2 in the virial factor (Graham et al. 2011; Park et al. 2012). The virial factor may differ by a factor of 2 depending on the bulge type (classical bulge and pseudo bulge; Ho & Kim 2014), which might be correlated to the systematics of the sample selection. One way to measure the virial factors of individual AGNs is via dynamically modeling the velocityresolved RM data (Pancoast et al. 2014a,b). Based on dynamical modeling results, Williams et al. (2018) reported uncertainties of 0.2-0.5 dex on the predictive distribution of the virial factor, corresponding to different definitions of the line width. We caution that the small scatter (e.g., 0.2 dex) may be due to the narrow range of parameter space spanned by their small sample. To derive the BH mass, the uncertainty of the virial factor is likely ≥0.3 dex altogether. Because the continuum-based method shares the same uncertainty in the virial factor as the RM method, the  $R_{\rm BLR}$ - $R_{\rm d}$  relation provides a promising method for measuring the BH mass closely if not equivalently to the accuracy of the RM method.

The single-epoch method is generally thought to be much more uncertain than RM due to the intrinsic scatter and the systematic bias of the *R*–*L* relation. The systematic deviation of the measured  $R_{\rm BLR}$  from the canonical R-L relation is discussed in Sects. 3 and 4.1. Dalla Bontà et al. (2020) recently provided the most accurate calibration of the single-epoch method with the RM database (Bentz & Katz 2015) and SDSS RM (Grier et al. 2017) samples. Their calibration empirically included the secondary dependence of the Eddington ratio, which resulted in an intrinsic scatter of 0.31 dex for the virial product ( $\propto R_{\rm BLR} \Delta V^2$ ) when the line dispersion (in contrast to the FWHM) is used. This scatter is equivalent to the intrinsic scatter we find for the  $R_{\rm BLR}$ - $R_{\rm d}$  relation ( $\lesssim 0.25$  dex), which will be the main contributor to the continuum-based virial product. We expect that the continuumbased method scatter can be reduced with future observations of the BLR and the dust-continuum size close in time, but we discuss the caveats in Sect. 4.3. The direct dust-continuum size measurement, which we have shown to be tightly linked to the BLR size, is a promising way to provide high-accuracy BH masses in the future (a more detailed discussion is provided in Sect. 5).

#### 4.3. Caveats

The primary goal of this work is to propose the idea of measuring the BH mass based on the dust-continuum size, particularly with time-efficient OI observations. The current calibration is not ideal because the BLR and dust continuum are not measured in the same AGN luminosity state. The line-width measurements in the lower part of Table 1 are collected from different epochs as well. This may introduce significant uncertainty on the BH

mass (Table 3) because the latter is  $\propto \Delta V^2$ . We therefore caution that the BH mass and Eddington ratio in Table 3 are only for the purpose of discussing the new method and are not rigorous measurements.

In practice, it may be difficult to measure the BLR and dust continuum size when they reflect the same luminosity state in order to calibrate the  $R_{\rm BLR}$ - $R_{\rm d}$  relation. It is more feasible to measure the BLR and the dust continuum sizes close in time (see also Sect. 5). In this way, the different time lags of the BLR and the hot dust will contribute to the intrinsic scatter of their size relation. The BLR size and the line width may show quicker and stronger variations than the dust continuum because the size of the BLR is 5–10 times smaller than the dust continuum. We expect a stronger averaging effect on the dust continuum as well. For an extreme example, the dust-continuum size may be correlated with a long-term average of the AGN luminosity over the previous several years, as discussed by Kishimoto et al. (2013) for NGC 4151. Future observations are important to quantify how much we can improve the  $R_{\rm BLR}$ - $R_{\rm d}$  relation from the first calibration provided in this work.

The current calibration of the  $R_{BLR}$ - $R_d$  relation is limited by the sample size. As briefly discussed in Sect. 3, various physical mechanisms may lead to the deviation of  $R \propto L^{0.5}$  for both the BLR and the hot dust. These deviations may reflect variations in BLR and hot dust structures, which may not necessarily follow each other. For example, the BLR radius may have a secondary dependence on the BH accretion rate (Du et al. 2015; Du & Wang 2019), while the dust sublimation radius does not depend on it (Barvainis 1987; Kishimoto et al. 2007). This difference means that the  $R_{\rm BLR}$ - $R_{\rm d}$  relation may depend on some secondary physical parameters, such as the accretion rate. No such dependence is found in the current sample (Sect. 3.3), but we cannot rule out the possibility that we are limited by the parameter space of the current sample. Following Du et al. (2015, Eq. (2)), we calculated the dimensionless accretion rate  $\dot{\mathcal{M}}$  and find that our targets span  $10^{-3} \le \dot{M} \le 200$ , with 23% of our targets falling in their super-Eddington regime (M > 3). We do not find a correlation between  $R_{\rm BLR}/R_{\rm d}$  and  $\mathcal{M}$ , but this correlation is worth revisiting with future larger samples that include more high-accretion rate AGNs.

#### 5. Prospects

The potential of OI observations in measuring the BLR and continuum of AGNs in the future is great. Current GRAVITY observations are limited to the brightest targets (K < 11). With the ongoing upgrade to significantly improve its sensitivity and sky coverage, GRAVITY+ will be capable of observing K < 13 AGNs in on-axis mode or even fainter AGNs in off-axis mode with a phase-reference source at  $\lesssim 30''$  (GRAVITY Collaboration 2022), enabling observations of thousands of AGNs from  $z \lesssim 0.2$  out to  $z \gtrsim 2$ .

Dust-continuum sizes are a side product of GRAVITY(+) spectroastrometry observations of the BLR if the AGN itself is bright enough to be the phase reference. Half of the AGN emission is split into the low-resolution beam combiner (or the 'fringe tracker'), which is used as the phase reference of the long-time exposure in the science channel to measure the BLR spectroastrometric signal (GRAVITY Collaboration 2017). The dust-continuum size can be measured from the visibility of the fringe-tracker data. Because the spectroastrometric measurement constrains the BLR geometry and dynamics and the BH mass for individual AGNs, we can use the simultaneous

Baskin, A., & Laor, A. 2018, MNRAS, 474, 1970

measurements of the BLR and continuum to calibrate the virial factor in Eq. (1) directly for  $R_d$  instead of  $R_{\rm BLR}$ . This approach will further improve the accuracy of BH masses from the continuum-based method.

GRAVITY can efficiently measure the dust continuum size, for instance, a  $\lesssim$ one-hour observation for one source with the current sensitivity (GRAVITY Collaboration et al., in prep.). We can place all AGN light into the fringe tracker so that the continuum method can measure the BH mass of AGNs a factor of two (or 0.75 mag) fainter than the spectroastrometry method. GRAVITY+ observations will enable measuring the dust continuum size and deriving the BLR size of a few hundred  $z \lesssim 0.2$  AGNs, including many sources with  $\lambda L_{\lambda}(5100~\text{Å}) > 10^{45}~\text{erg s}^{-1}$ . They will be crucial for understanding the dependence of BLR properties and the BH accretion on the AGN properties.

## 6. Summary

We collected 42 AGNs with dust-continuum size measurements from RM and/or OI observations. The BLR size based on  $H\beta$  RM measurements of 26 of these AGNs are available. We find close linear relations between the BLR and dust-continuum radius with an intrinsic scatter of only 0.25 dex. The dust-continuum radius measured by OI is about twice as large as that measured by RM. Dust-continuum radii measured by RM and OI are about five and ten times the radius of the BLR, respectively. We provided simple scaling relations to derive the BLR radius based on the dust-continuum radius, measured with RM and OI separately. For the remaining 16 AGNs, we calculated the BLR radii, BH masses, and Eddington ratios using the  $R_{\rm BLR}$ - $R_{\rm d}$  relations. We find that these AGNs consistently follow the BLR R-L relation of previous RM and GRAVITY measurements. All targets significantly below the Bentz et al. (2013) relation show a high Eddington ratio.

The accuracy of the continuum-based BH mass is comparable to that of the integrated broad emission line RM measurements because the primary uncertainty comes from the virial factor. The primary goal of this paper is to propose a new method of measuring the BH mass based on the dust-continuum size. We discussed the caveats of the method in detail. More continuum observations close in time with BLR measurements will be essential for studying the  $R_{\rm BLR}-R_{\rm d}$  relation better in the future. In particular, it is important to test whether luminous AGNs with large BLRs show a different  $R_{\rm BLR}-R_{\rm d}$  relation compared to their low-luminosity counterparts. With its improved sensitivity, GRAVITY+ will be powerful in improving the continuum-based method and in efficiently measuring the BH mass for a large sample of AGNs in the low-redshift Universe using this method.

Acknowledgements. We thank the anonymous referees for their careful reading and suggestions that helped to improve this manuscript. This project has received funding from the European Union's Horizon 2020 research and innovation programme under grant agreement No. 101004719. This research has made use of the NASA/IPAC Extragalactic Database (NED) which is operated by the California Institute of Technology, under contract with the National Aeronautics and Space Administration. This research has made use of the SIMBAD database, operated at CDS, Strasbourg, France.

## References

```
Baribaud, T., Alloin, D., Glass, I., & Pelat, D. 1992, A&A, 256, 375
Barth, A. J., Nguyen, M. L., Malkan, M. A., et al. 2011, ApJ, 732, 121
Barvainis, R. 1987, ApJ, 320, 537
```

```
Bentz, M. C., & Katz, S. 2015, PASP, 127, 67
Bentz, M. C., Denney, K. D., Grier, C. J., et al. 2013, ApJ, 767, 149
Bentz, M. C., Street, R., Onken, C. A., & Valluri, M. 2021, ApJ, 906, 50
Blandford, R. D., & McKee, C. F. 1982, ApJ, 255, 419
Boizelle, B. D., Barth, A. J., Walsh, J. L., et al. 2019, ApJ, 881, 10
Boroson, T. A., & Green, R. F. 1992, ApJS, 80, 109
Burtscher, L., Meisenheimer, K., Tristram, K. R. W., et al. 2013, A&A, 558,
   A149
Clavel, J., Wamsteker, W., & Glass, I. S. 1989, ApJ, 337, 236
Collin, S., Kawaguchi, T., Peterson, B. M., & Vestergaard, M. 2006, A&A, 456,
Dalla Bontà, E., Peterson, B. M., Bentz, M. C., et al. 2020, ApJ, 903, 112
Davis, T. A. 2014, MNRAS, 443, 911
Denney, K. D., De Rosa, G., Croxall, K., et al. 2014, ApJ, 796, 134
Dong, X. Y., Wu, X.-B., Ai, Y. L., et al. 2018, AJ, 155, 189
Du, P., & Wang, J.-M. 2019, ApJ, 886, 42
Du, P., Hu, C., Lu, K.-X., et al. 2015, ApJ, 806, 22
Du, P., Brotherton, M. S., Wang, K., et al. 2018, ApJ, 869, 142
Ferrarese, L., & Merritt, D. 2000, ApJ, 539, L9
Fonseca Alvarez, G., Trump, J. R., Homayouni, Y., et al. 2020, ApJ, 899, 73
Foreman-Mackey, D., Hogg, D. W., Lang, D., & Goodman, J. 2013, PASP, 125,
Gebhardt, K., Bender, R., Bower, G., et al. 2000, ApJ, 539, L13
Glass, I. S. 1992, MNRAS, 256, 23P
Goodrich, R. W. 1989, ApJ, 340, 190
Graham, A. W., Onken, C. A., Athanassoula, E., & Combes, F. 2011, MNRAS,
   412, 2211
GRAVITY Collaboration (Abuter, R., et al.) 2017, A&A, 602, A94
GRAVITY Collaboration (Abuter, R., et al.) 2022, A&A, 665, A75
GRAVITY Collaboration (Amorim, A., et al.) 2020a, A&A, 643, A154
GRAVITY Collaboration (Amorim, A., et al.) 2021a, A&A, 654, A85
GRAVITY Collaboration (Amorim, A., et al.) 2021b, A&A, 648, A117
GRAVITY Collaboration (Dexter, J., et al.) 2020b, A&A, 635, A92
GRAVITY Collaboration (Sturm, E., et al.) 2018, Nature, 563, 657
Greene, J. E., & Ho, L. C. 2005, ApJ, 630, 122
Grier, C. J., Martini, P., Watson, L. C., et al. 2013, ApJ, 773, 90
Grier, C. J., Trump, J. R., Shen, Y., et al. 2017, ApJ, 851, 21
Hicks, E. K. S., & Malkan, M. A. 2008, ApJS, 174, 31
Ho, L. C., & Kim, M. 2014, ApJ, 789, 17
Huang, Y.-K., Hu, C., Zhao, Y.-L., et al. 2019, ApJ, 876, 102
Jones, D. H., Read, M. A., Saunders, W., et al. 2009, MNRAS, 399, 683
Kaspi, S., Smith, P. S., Netzer, H., et al. 2000, ApJ, 533, 631
Kawaguchi, T., & Mori, M. 2010, ApJ, 724, L183
Kishimoto, M., Hönig, S. F., Beckert, T., & Weigelt, G. 2007, A&A, 476,
Kishimoto, M., Hönig, S. F., Antonucci, R., et al. 2009, A&A, 507, L57
Kishimoto, M., Hönig, S. F., Antonucci, R., et al. 2011, A&A, 527, A121
Kishimoto, M., Hönig, S. F., Antonucci, R., et al. 2013, ApJ, 775, L36
Kishimoto, M., Anderson, M., ten Brummelaar, T., et al. 2022, ApJ, 940, 28
Kokubo, M., & Minezaki, T. 2020, MNRAS, 491, 4615
Kollatschny, W., & Fricke, K. J. 1985, A&A, 146, L11
Korista, K. T., & Goad, M. R. 2004, ApJ, 606, 749
Koshida, S., Minezaki, T., Yoshii, Y., et al. 2014, ApJ, 788, 159
Koss, M., Trakhtenbrot, B., Ricci, C., et al. 2017, ApJ, 850, 74
Leftley, J. H., Tristram, K. R. W., Hönig, S. F., et al. 2021, ApJ, 912, 96
Lira, P., Arévalo, P., Uttley, P., McHardy, I., & Breedt, E. 2011, MNRAS, 415,
   1290
Lira, P., Arévalo, P., Uttley, P., McHardy, I. M. M., & Videla, L. 2015, MNRAS,
   454, 368
Lub, J., & de Ruiter, H. R. 1992, A&A, 256, 33
Mandal, A. K., Rakshit, S., Kurian, K. S., et al. 2018, MNRAS, 475, 5330
Mandal, A. K., Rakshit, S., Stalin, C. S., et al. 2021a, MNRAS, 501, 3905
Mandal, A. K., Schramm, M., Rakshit, S., et al. 2021b, MNRAS, 508, 5296
Marconi, A., Maiolino, R., & Petrov, R. G. 2003, Ap&SS, 286, 245
Marin, F., Hutsemékers, D., Agís González, B., et al. 2019, in SF2A-2019:
   Proceedings of the Annual meeting of the French Society of Astronomy and
   Astrophysics, eds. P. Di Matteo, O. Creevey, A. Crida, et al.
Martínez-Aldama, M. L., Czerny, B., Kawka, D., et al. 2019, ApJ, 883, 170
Mejía-Restrepo, J. E., Lira, P., Netzer, H., Trakhtenbrot, B., & Capellupo, D. M.
   2018, Nat. Astron., 2, 63
Minezaki, T., Yoshii, Y., Kobayashi, Y., et al. 2004, ApJ, 600, L35
Minezaki, T., Yoshii, Y., Kobayashi, Y., et al. 2019, ApJ, 886, 150
Nardini, E., Reeves, J. N., Gofford, J., et al. 2015, Science, 347, 860
Netzer, H. 1990, in Active Galactic Nuclei, eds. R. D. Blandford, H. Netzer, L.
   Woltjer, T. J. L. Courvoisier, & M. Mayor, 57
Oknyanskij, V. L., Lyuty, V. M., Taranova, O. G., & Shenavrin, V. I. 1999,
   Astron. Lett., 25, 483
```

```
Oknyansky, V. L., Gaskell, C. M., & Shimanovskaya, E. V. 2015, Odessa Astron.
   Publ., 28, 175
Onishi, K., Iguchi, S., Davis, T. A., et al. 2017, MNRAS, 468, 4663
Onken, C. A., & Peterson, B. M. 2002, ApJ, 572, 746
Onken, C. A., Ferrarese, L., Merritt, D., et al. 2004, ApJ, 615, 645
Onken, C. A., Valluri, M., Brown, J. S., et al. 2014, ApJ, 791, 37
Onori, F., Ricci, F., La Franca, F., et al. 2017, MNRAS, 468, L97
Pan, X., Zhou, H., Yang, C., et al. 2021, ApJ, 912, 118
Pancoast, A., Brewer, B. J., & Treu, T. 2014a, MNRAS, 445, 3055
Pancoast, A., Brewer, B. J., Treu, T., et al. 2014b, MNRAS, 445, 3073
Park, D., Kelly, B. C., Woo, J.-H., & Treu, T. 2012, ApJS, 203, 6
Peterson, B. M. 1993, PASP, 105, 247
Peterson, B. M. 2014, Space Sci. Rev., 183, 253
Peterson, B. M., Wanders, I., Bertram, R., et al. 1998, ApJ, 501, 82
Peterson, B. M., Ferrarese, L., Gilbert, K. M., et al. 2004, ApJ, 613, 682
Petrov, R. G., Malbet, F., Richichi, A., et al. 2001, Comptes Rendus Phys., 2,
   67
Planck Collaboration XIII. 2016, A&A, 594, A13
Pozo Nuñez, F., Haas, M., Chini, R., et al. 2014, A&A, 561, L8
Pozo Nuñez, F., Ramolla, M., Westhues, C., et al. 2015, A&A, 576, A73
Prieto, A., Rodríguez-Ardila, A., Panda, S., & Marinello, M. 2022, MNRAS,
Probst, M. A., & Kollatschny, W. 2020, Contrib. Astron. Obs. Skalnate Pleso,
   50.360
Ramolla, M., Haas, M., Westhues, C., et al. 2018, A&A, 620, A137
Rashed, Y. E., Eckart, A., Valencia-S., M., et al. 2015, MNRAS, 454, 2918
Rees, M. J., Silk, J. I., Werner, M. W., & Wickramasinghe, N. C. 1969, Nature,
Saglia, R. P., Opitsch, M., Erwin, P., et al. 2016, ApJ, 818, 47
Senarath, M. R., Brown, M. J. I., Cluver, M. E., et al. 2021, MNRAS, 503,
Shangguan, J., Ho, L. C., & Xie, Y. 2018, ApJ, 854, 158
Shankar, F., Bernardi, M., Richardson, K., et al. 2019, MNRAS, 485, 1278
Shapovalova, A. I., Popović, L. Č., et al. 2019, MNRAS, 485, 4790
Shen, Y. 2013, Bull. Astron. Soc. India, 41, 61
Shen, Y., & Ho, L. C. 2014, Nature, 513, 210
Sitko, M. L., Sitko, A. K., Siemiginowska, A., & Szczerba, R. 1993, ApJ, 409,
Sobrino Figaredo, C., Haas, M., Ramolla, M., et al. 2020, AJ, 159, 259
Stalin, C. S., Jeyakumar, S., Coziol, R., Pawase, R. S., & Thakur, S. S. 2011,
   MNRAS, 416, 225
Suganuma, M., Yoshii, Y., Kobayashi, Y., et al. 2006, ApJ, 639, 46
Swain, M., Vasisht, G., Akeson, R., et al. 2003, ApJ, 596, L163
Thomas, J., Saglia, R. P., Bender, R., et al. 2004, MNRAS, 353, 391
Vestergaard, M., & Peterson, B. M. 2006, ApJ, 641, 689
Wang, J.-M., Du, P., Brotherton, M. S., et al. 2017, Nat. Astron., 1, 775
Williams, P. R., Pancoast, A., Treu, T., et al. 2018, ApJ, 866, 75
Wittkowski, M., Kervella, P., Arsenault, R., et al. 2004, A&A, 418, L39
Woo, J.-H., Treu, T., Barth, A. J., et al. 2010, ApJ, 716, 269
Zheng, X. Z., Xia, X. Y., Mao, S., Wu, H., & Deng, Z. G. 2002, AJ, 124,
```

- <sup>1</sup> Max Planck Institute for Extraterrestrial Physics (MPE), Giessenbachstr.1, 85748 Garching, Germany
- <sup>2</sup> LESIA, Observatoire de Paris, Université PSL, CNRS, Sorbonne Université, Univ. Paris Diderot, Sorbonne Paris Cité, 5 Place Jules Janssen, 92195 Meudon, France
- <sup>3</sup> I. Institute of Physics, University of Cologne, Zülpicher Straße 77, 50937 Cologne, Germany
- Departments of Physics and Astronomy, Le Conte Hall, University of California, Berkeley, CA 94720, USA
- Department of Physics and Astronomy, University of Southampton, Southampton SO17 1BJ, UK
- <sup>6</sup> Department of Astrophysics & Atmospheric Sciences, Kyoto Sangyo University, Kamigamo-motoyama, Kita-ku, Kyoto 603-8555, Japan
- Université Côte d'Azur, Observatoire de la Côte d'Azur, CNRS, Laboratoire Lagrange, Boulevard de l'Observatoire, 06304 Nice Cedex 4, France
- School of Physics and Astronomy, Tel Aviv University, Tel Aviv 69978, Israel
- <sup>9</sup> Univ. Grenoble Alpes, CNRS, IPAG, 38000 Grenoble, France
- Center for Computational Astrophysics, Flatiron Institute, 162 5th Ave., New York, NY 10010, USA
- <sup>11</sup> European Southern Observatory, Casilla 19001, Santiago 19, Chile
- <sup>2</sup> European Southern Observatory, Karl-Schwarzschild-Str. 2, 85748 Garching, Germany
- <sup>13</sup> Sterrewacht Leiden, Leiden University, Postbus 9513, 2300, RA Leiden, The Netherlands
- Max Planck Institute for Radio Astronomy, Auf dem Hügel 69, 53121 Bonn, Germany
- <sup>15</sup> Universidade de Lisboa Faculdade de Ciências, Campo Grande, 1749-016 Lisboa, Portugal
- <sup>16</sup> Faculdade de Engenharia, Universidade do Porto, Rua Dr. Roberto Frias, 4200-465 Porto, Portugal
- 17 CENTRA Centro de Astrofísica e Gravitação, IST, Universidade de Lisboa, 1049-001 Lisboa, Portugal
- <sup>18</sup> Max Planck Institute for Astronomy, Königstuhl 17, 69117 Heidelberg, Germany
- <sup>19</sup> Instituto de Astrofísica de Canarias (IAC), E-38205 La Laguna, Tenerife, Spain
- Department of Astrophysical & Planetary Sciences, JILA, University of Colorado, Duane Physics Bldg., 2000 Colorado Ave., Boulder, CO 80309, USA
- <sup>21</sup> Research School of Astronomy and Astrophysics, Australian National University, Bart Bok Rd, Canberra, ACT 2611, Australia
- Retired c/o T.L. Turner, 205 South Prospect Street, Granville, OH 43023, USA